

Self-supervised Multi-future Occupancy Forecasting for Autonomous Driving

Bernard Lange¹, Masha Itkina¹, Jiachen Li², and Mykel J. Kochenderfer¹

Abstract—Environment prediction frameworks are critical for the safe navigation of autonomous vehicles (AVs) in dynamic settings. LiDAR-generated occupancy grid maps (L-OGMs) offer a robust bird’s-eye view for the scene representation, enabling self-supervised joint scene predictions while exhibiting resilience to partial observability and perception detection failures. Prior approaches have focused on deterministic L-OGM prediction architectures within the grid cell space. While these methods have seen some success, they frequently produce unrealistic predictions and fail to capture the stochastic nature of the environment. Additionally, they do not effectively integrate additional sensor modalities present in AVs. Our proposed framework performs stochastic L-OGM prediction in the latent space of a generative architecture and allows for conditioning on RGB cameras, maps, and planned trajectories. We decode predictions using either a single-step decoder, which provides high-quality predictions in real-time, or a diffusion-based batch decoder, which can further refine the decoded frames to address temporal consistency issues and reduce compression losses. Our experiments on the nuScenes and Waymo Open datasets show that all variants of our approach qualitatively and quantitatively outperform prior approaches.

I. INTRODUCTION

Accurate environment prediction algorithms are essential for autonomous vehicle (AV) navigation in urban settings. Experienced drivers understand scene semantics and recognize the intents of other agents to anticipate their trajectories and safely navigate to their destination. To replicate this process in AVs, many environment prediction approaches have been proposed, employing different environment representations and modeling assumptions [1]–[7].

The modern AV stack comprises a mixture of expert-designed and learned modules, such as 3D object detection, tracking, and motion forecasting, each developed independently. In the case of learned systems, development involves using curated labels provided by human annotators and other perception systems. For environment reasoning, object-based prediction algorithms are often used, which rely on the perception system to create a vectorized representation of the scene with defined agents and environmental features [4], [8]. However, this approach has multiple limitations. First, it often generates marginalized future trajectories for each individual agent, rather than a holistic scene prediction including agent interactions, which complicates integration with planning modules [9]. Second, this approach does not take sensor measurements into account and depends solely on

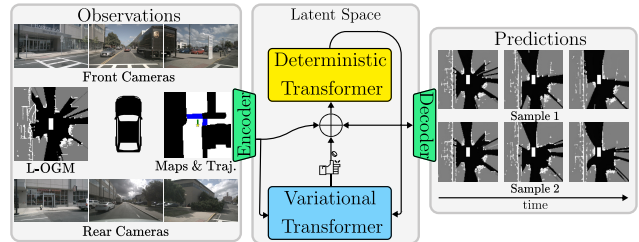


Fig. 1: Latent Occupancy Prediction (LOPR) is a self-supervised stochastic prediction framework that forecasts occupancy grid maps within the latent space of a generative model. It consists of deterministic and variational transformer modules conditioned on occupancy grids, images, maps, and the planned trajectory. LOPR forecasts multiple plausible futures for the entire scene.

object detection algorithms that may fail in suboptimal conditions [10], [11]. Third, reliance on labeled data, sourced from both human annotators and perception systems, constrains the dataset size and incurs higher costs. These drawbacks render the AV stack susceptible to cascading failures and can lead to poor generalization in unforeseen scenarios. Such limitations underscore the need for complementary environment modeling approaches that do not rely on error-prone and expensive labeling schemes.

In response to these challenges, occupancy grid maps generated from LiDAR measurements (L-OGMs) have gained popularity as a form of scene representation for prediction. The popularity is due to their minimal data preprocessing requirements, eliminating the need for manual labeling, the ability to model the joint prediction of the scene with an arbitrary number of agents, and robustness to partial observability and detection failures [1], [2]. We focus on ego-centric L-OGM prediction generated using uncertainty-aware occupancy state estimation approaches [12]. Due to its generality and ability to scale with unlabeled data, we hypothesize that L-OGM prediction alongside RGB video prediction could also serve as an unsupervised pre-training objective, i.e., a foundational model, for autonomous driving.

The task of L-OGM prediction is typically framed as self-supervised sequence-to-sequence learning. ConvLSTM-based architectures have been used predominantly in previous work for this task due to their ability to handle spatiotemporal sequences [1]–[3], [13]. These approaches are optimized end-to-end in grid cell space, do not account for the stochasticity present in the scene, and neglect other available modalities, e.g., RGB cameras around the vehicle, maps, and the planned trajectory. As a result, they often suffer from unrealistic and blurry predictions.

In this work, we address the limitations of previous

¹Department of Aeronautics and Astronautics, Stanford University, Stanford, CA 94305, USA {blange, mitkina, mykel}@stanford.edu

²Department of Electrical and Computer Engineering, University of California, Riverside, Riverside, CA 92507, USA jiachen.li@ucr.edu

approaches by proposing a stochastic L-OGM prediction framework that operates within the latent space of a generative model. Generative models are known for providing a compressed representation, while producing high-quality samples [14], [15]. With the use of generative models, we can minimize redundancies in the representation, allowing the prediction network to focus computation on the most critical aspects of the task [16].

Within the latent space trained on L-OGMs, our framework employs an autoregressive transformer-based architecture, comprising both deterministic and variational decoder models. Both modules are conditioned on past L-OGMs encodings and other modalities if available, such as camera images, maps, and the planned trajectory, as shown in Fig. 1. Predictions are decoded using a single-step decoder, which provides high-quality predictions in real-time that optionally can be refined with a diffusion-based batch decoder. The diffusion-based batch decoder addresses temporal consistency issues associated with single-step decoders [17] and mitigates compression losses by conditioning on prior rasterized L-OGMs, at the cost of real-time feasibility.

Experiments on nuScenes [18] and the Waymo Open Dataset [19] show quantitative and qualitative improvements over baseline approaches. Our framework forecasts diverse futures and infers unobserved agents. It also leverages other sensor modalities for more accurate predictions, such as observing oncoming vehicles in a camera feed beyond the visible region of the L-OGMs. Our contributions are:

- We introduce a framework called **Latent Occupancy Prediction (LOPR)** for stochastic L-OGM prediction in the latent space of a generative model conditioned on other sensor modalities, such as RGB cameras, maps and the planned AV trajectory.
- We propose a variational-based transformer model that captures the stochasticity of the surrounding scene while remaining real-time feasible.
- We define a diffusion-based batch decoder that refines single-frame decoder outputs to address temporal consistency issues and reduce compression losses.
- Through experiments on nuScenes [18] and the Waymo Open Dataset [19], we show that all variations of LOPR outperform prior L-OGM prediction methods.

II. RELATED WORK

OGM Prediction. The majority of prior work in OGM prediction generates OGMs with LiDAR measurements (L-OGMs) and uses an adaptation on the recurrent neural network (RNN) with convolutions [20], [21]. Dequaire *et al.* [22] tracked objects through occlusions and predicted future binary OGMs with an RNN and a spatial transformer. Schreiber *et al.* [13] provided dynamic occupancy grid maps (DOGMas) with cell-wise velocity estimates as input to a ConvLSTM for environment prediction from a stationary platform. Schreiber *et al.* [23] then extended this work to forecast DOGMas in a moving ego-vehicle setting. Mohajerin *et al.* [24] applied a difference learning approach to predict OGMs as seen from the coordinate

frame of the first observed time step. Itkina *et al.* [1] used the PredNet ConvLSTM architecture [25] to achieve ego-centric OGM prediction. Lange *et al.* [2] reduced the blurring and the gradual disappearance of dynamic obstacles in the predicted grids by developing an attention augmented ConvLSTM mechanism. Concurrently, Toyungyernsub *et al.* [3] addressed obstacle disappearance with a double-prong framework assuming knowledge of the static and dynamic obstacles. An alternative approach predicts occupancy grid maps from vectorized object data [6] or a mixture of vectorized object data and sensor measurements [26]. Similar to representations in common trajectory prediction techniques, these methods require substantial labeling efforts [27]–[29]. Unlike prior work, we perform self-supervised multi-future L-OGM predictions in the latent space of generative models conditioned on additional sensor modalities without the need for manual labeling.

Representation Learning in Robotics and Autonomous Driving. The objective of representation learning is to identify low-dimensional representations that make it easier to achieve the desired performance on a task. Many robotics applications use architectures such as the autoencoder (AE) [30], the variational autoencoder (VAE) [15], the generative adversarial network (GAN) [14], and the vector quantized variational autoencoder (VQ-VAE) [31]. Latent spaces have been used to learn latent dynamics from pixels [32], output video predictions [33], generate trajectories [34], and learn autonomous driving neural simulators [17], [35]. Large-scale video prediction architectures have used discrete representations provided by the VQ-VAE [31] with a causal transformer [17], [36], [37]. However, these models remain prohibitively expensive to train and sample from. We present a method that performs multi-future L-OGM prediction entirely in the latent space of generative models in real time.

III. LOPR: LATENT OCCUPANCY PREDICTION

We propose the Latent Occupancy Prediction (LOPR) framework designed to generate stochastic scene predictions in the form of L-OGMs. The model separates the task into (1) learning an L-OGM representation and (2) making predictions in the latent space of a generative model. In the representation learning phase, a VAE-GAN is trained to learn an L-OGM latent space. During the prediction stage, our framework uses an autoregressive transformer-based architecture, comprising both deterministic and variational decoder models. At each time step, a sample is drawn from the variational transformer and then passed to the deterministic transformer to forecast the next L-OGM embedding. Predictions are conditioned on past L-OGMs encodings and other available modalities, such as camera images, maps, and the planned trajectory. The encoders for maps and planned trajectories are trained alongside the prediction framework, while for the image encoder, we use a pre-trained DINOv2-based model [38]. Predictions are decoded using a single-step decoder, which provides high-quality predictions in real-time

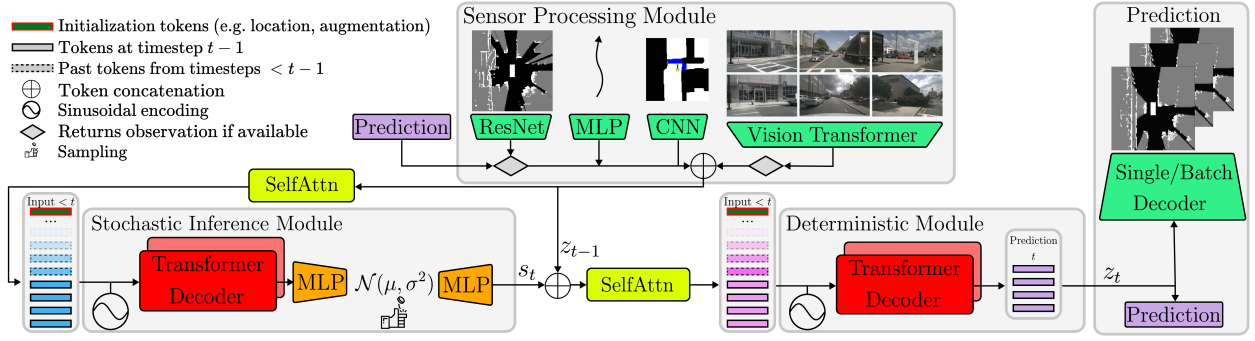


Fig. 2: The LOPR framework, comprising sensor processing, stochastic inference, and prediction modules. The sensor processing module encodes all sensor modalities. The L-OGM and RGB camera encoders are pretrained as described in Section III-A and in Section III-D. The inference module captures the scene’s stochasticity (Section III-B). In the prediction module, we forecast the next time step’s L-OGM embedding. At each time step, the most recent predictions are autoregressively provided to the inference and prediction modules.

that optionally can be refined with a diffusion-based batch decoder. Fig. 2 summarizes the framework.

A. Representation Learning

The latent space for L-OGMs is obtained by training an encoder and a decoder. Given an L-OGM grid $x \in \mathbb{R}^{H \times W}$ with size (H, W) , the encoder outputs a low-dimensional latent representation $z \in \mathbb{R}^{c \times h \times w}$ with dimensions (h, w) and depth c . This representation is reconstructed by a decoder to $\hat{x} \in \mathbb{R}^{H \times W}$. The framework integrates concepts from β -VAE and GAN [35], [39]. In β -VAE, the objective consists of the reconstruction and regularization losses:

$$\mathcal{L}_{\text{VAE}} = -\mathbb{E}_{q(z|x)} [\log p(x|z)] + \beta D_{\text{KL}}(q(z|x) || p(z)), \quad (1)$$

where $q(z|x)$ and $p(x|z)$ are the outputs of the encoder and decoder respectively, $p(z)$ is the unit Gaussian prior, and D_{KL} represents the Kullback-Leibler divergence. The reconstruction loss is an average of the perceptual loss [40] and the mean squared error. In the GAN step, the same decoder serves as the generator, and a discriminator classifies whether samples originate from the training set. This framework uses minimax optimization for the following objective [14]:

$$\mathcal{L}_{\text{GAN}} = \mathbb{E}_{x \sim p_{\text{data}}} [\log \mathcal{D}(x)] + \mathbb{E}_{\hat{x} \sim p_{\text{model}}} [\log (1 - \mathcal{D}(\hat{x}))], \quad (2)$$

where \mathcal{D} is the discriminator. The final loss is $\mathcal{L}_{\text{rep}} = \mathcal{L}_{\text{VAE}} + \mathcal{L}_{\text{GAN}}$ and follows the implementation described by Kim *et al.* [35] and Karras *et al.* [41].

B. Stochastic L-OGM Sequence Prediction

Given the pre-trained L-OGM latent space, we train a stochastic sequence prediction network that receives a history of observations and outputs a distribution over a potential future embedding $p_{\theta}(z_t | z_{<t})$, where $z_{<t}$ represents the compressed L-OGM representations over the last t time steps, and θ are the network weights. The environment prediction task is inherently multimodal, and the latent vectors contributing to this stochasticity are unobservable. We introduce a variable s_t to capture this stochasticity at timestep t of the sequence and extend our model to

$p_{\theta}(z_t | z_{<t}, s_{\leq t})$ [33]. During training, we extract the true posterior using an inference network $s_t \sim q_{\phi}(s_t | z_{\leq t})$ which has access to the z_t , representation of L-OGM at timestep t . While at test time, we sample from a learned prior $s_t \sim p_{\gamma}(s_t | z_{<t})$ as we are attempting to predict z_t . This process is autoregressively repeated for T_F future steps assuming access for T_O past observations. The framework is optimized using the variational lower bound objective [15]:

$$\mathcal{L} = - \sum_{t=T_O}^{T_O+T_F} \mathbb{E}_{q_{\phi}(s_{\leq t}|z_{\leq t})} [\log p_{\theta}(z_t | z_{<t}, s_{\leq t})] + D_{\text{KL}}(q_{\phi}(s_t | z_{\leq t}) || p_{\gamma}(s_t | z_{<t})), \quad (3)$$

where the prediction network and prior autoregressively receive previous predicted embeddings, whereas the posterior takes in only the ground truth.

LOPR is implemented using a transformer-based architecture, comprising a deterministic decoder \mathcal{P}_{θ} and two inference networks \mathcal{Q}_{ϕ} and \mathcal{Q}_{γ} for the prior and posterior, respectively. The positional information is provided through a sinusoidal positional encoding [36]. At each time step t , s_t is sampled from the inference network \mathcal{Q} , which outputs the parameters of the Gaussian distribution:

$$\mu, \sigma = \mathcal{Q}(z_{\leq \text{or } <t}) \quad (4)$$

$$s_t \sim \mathcal{N}(\mu, \sigma^2), \quad (5)$$

where s_t is drawn from \mathcal{Q}_{ϕ} at test time and from \mathcal{Q}_{γ} at training time, as explained above. Then z_{t-1} is attended with s_t and provided to the deterministic decoder where all past representations are incorporated:

$$z_t = \mathcal{P}_{\theta}(\text{SelfAttn}(z_{<t}, s_{\leq t})). \quad (6)$$

In the above operations, each $z_t \in \mathbb{R}^{c \times h \times w}$ is split along its spatial dimensions into k patches, which are then flattened [42]. Each token has dimension $\frac{chw}{k}$, thereby also facilitating spatial attention and optimizing the parameter count in the attention layer. This operation is applied to both the deterministic decoder and the inference networks. In the final step, the predicted compressed representations are concatenated, reshaped back to their original dimensions, and then provided to the decoder from Section III-A.

C. Diffusion-based Batch Decoder

We can decode each z_t independently using the single-frame decoder outlined in Section III-A to obtain high-quality predictions in real time. However, this approach can lead to poor temporal consistency and compression losses [17]. They manifest as unrealistic changes in the distribution of occupied cells over time and poor pixel-wise accuracy, particularly in the first predicted frames that should retain most of the static details from the observations.

We address these issues by refining $\hat{x}_{t-\Delta:t}$ from the single-frame decoder in batches with a diffusion-based batch decoder, where Δ is the number of frames. The batch decoder is conditioned on decoded frames $\hat{x}_{t-\Delta:t}$ and a rasterized frame preceding the sequence $x_{t-\Delta-1}$. We follow a standard video diffusion formulation that uses a 3D-UNet as a denoising model and minimizes the mean-squared error between the predicted and ground truth noises [43]. The model is trained to refine the decoded ground truth frames $\hat{x}_{t-\Delta:t}$ to more closely match $x_{t-\Delta:t}$. At test time, the decoded frames and preceding rasterized frames are reconstructions of the predicted embeddings prior, except for the first prediction, where the preceding frame is a rasterized observation.

D. Conditioning on Other Sensor Modalities

LOPR can be conditioned on maps, the planned trajectory, and observed RGB camera images. We assume access to maps for the entire planned trajectory. Each input modality is first embedded as described below and then integrated into the framework using the self-attention mechanism before being provided to deterministic and inference networks.

Maps and Planned AV Trajectory. The map $m \in \mathbb{R}^{3 \times W \times H}$ comprises the drivable area, stop lines, and pedestrian crossings within the ego frame, represented using a rasterized format. The planned trajectory $tr \in \mathbb{R}^{3 \times T}$ includes position (x, y, z) for the entire sequence, normalized with respect to the ego position. Maps and the planned trajectory are processed using convolutional and fully connected networks.

RGB Camera. The camera observation, denoted as $c_t \in \mathbb{R}^{N \times 3 \times W \times H}$, encompasses views from N RGB cameras surrounding the vehicle. They offer important semantic information not available in L-OGMs. They can: 1) distinguish whether occupied cells are dynamic agents (like cars), including their type and orientation, or static environmental elements, and 2) provide insights into the state of the environment beyond the area observed in the fixed-size L-OGM. Incorporating RGB inputs into the self-supervised perception task is challenging due to the limited size of the AV perception datasets. To address this, we use the DINOv2 [38] backbone and pre-train the module on a short deterministic prediction task while conditioning on observed L-OGMs and planned trajectory embeddings. This approach encourages the extraction of visual information useful for downstream stochastic prediction.

Fig. 3 shows the image processing module \mathcal{I}_β . Each image is embedded using a DINOv2 backbone. It is followed by a series of transformer modules: 1) The image layer, which aggregates tokens from a single view. 2) The spatial layer,

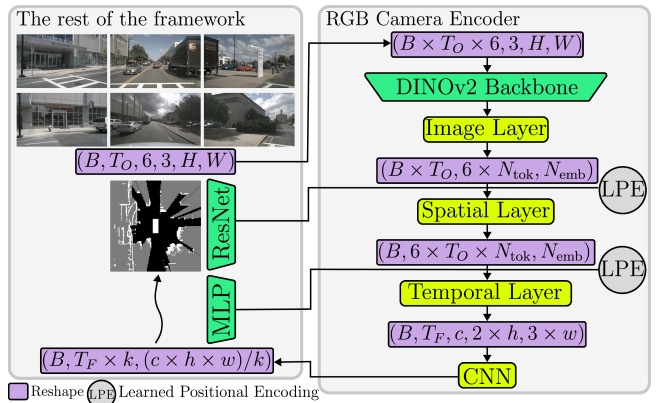


Fig. 3: RGB camera data is processed through the pre-trained DINOv2 backbone, subsequently passing through a series of transformers. These transformers aggregate information within each view (image layer), across different views (spatial layer), and throughout all observed timesteps. The spatial and temporal layers also include the learned positional embedding and are conditioned on the L-OGM embeddings and the planned trajectory, respectively.

which collects embeddings from each perspective around the vehicle along with a corresponding L-OGM embedding. 3) The temporal layer, which aggregates information across all observed time steps and the planned AV trajectory. Finally, the tokens from each time step are concatenated along the spatial dimensions and then processed through a convolutional layer to produce z_{cam} . The output tokens are then segmented back into patches, flattened, and integrated into the framework using the self-attention mechanism.

E. Conditioning on Other Information

Locations. Considering the diversity of locations in nuScenes [18], we append a one-hot location encoding (Singapore or USA) to the start of the observations sequence.

Sequence Augmentation. The open-source perception datasets are relatively small compared to vectorized trajectory datasets. To increase the number of samples, we implement a series of augmentations (e.g. mirror reflections, rotations, and reversing the sequence). Recognizing that these augmentations might adversely affect the prediction correctness (e.g. potentially resulting in predictions that do not adhere to driving rules), we attach a one-hot encoding of the augmentation type at the beginning of the sequence.

F. Prediction Extrapolation

We extend the prediction horizon at test time using a sliding-window approach, treating the last predicted frames as observations and repeating the process. However, unlike maps and planned trajectory modalities, we neither have access to nor predict future camera observations. Hence, we randomly drop out the image embeddings enabling robust extrapolation beyond the training-time prediction horizon.

IV. EXPERIMENTS

We evaluate our framework by analyzing the pre-trained latent space, evaluating its performance in environment prediction tasks, and examining the impact of additional sensor modalities on the predictions quality.

A. Dataset

We use the nuScenes Dataset [18] and the Waymo Open Dataset [19]. nuScenes contains 5.5 hours of data collected in Boston and Singapore. Waymo Open Dataset [19] provides 6.4 hours of data compiled in San Francisco, Phoenix, and Mountain View. Both datasets include measurements from RGB cameras around the vehicle, LiDAR(s), and maps.

Data Representation: We generate L-OGMs in the ego vehicle frame using a ground-segmented LiDAR point cloud. The OGM dimensions are $H \times W = 128 \times 128$ with a 0.3 m resolution, corresponding to a $42.7\text{ m} \times 42.7\text{ m}$ grid. RGB images and maps are downscaled to 224×224 and 128×128 respectively. During sequence prediction training, we provide 5 past L-OGMs (0.5 s) as observations alongside other sensor modalities, and forecast for 15 future frames (1.5 s) at 10 Hz. We also extend the prediction horizon to 30 frames (3.0 s) to evaluate the extrapolation capabilities of our framework.

B. Architecture and Training Details

Architectures. We incorporate a convolutional network for all modules except the transformer-based ones and the trajectory encoder. The discriminator architecture is multi-scale and multi-patch, inspired by prior work [44]. The dimension of the latent vector is set at $z \in \mathbb{R}^{64 \times 4 \times 4}$ which is split in 4 patches resulting in the flattened embedding size of 256. For the prediction network, the decoder and variational modules each consist of 6 layers and 6 heads, collectively comprising 16.1 million parameters. The image module employs a DINOv2 ViT-S/14 backbone [38]. Within this module, the image, spatial, and temporal layers comprise 1, 4, and 4 layers, respectively, each with 4 heads. The total number of parameters for the image head is 27.4M. For the diffusion-based decoder, we leverage an implementation by HuggingFace [45]. In the results section, we use a single-step decoder, unless stated otherwise.

Model Training. We used the AdamW optimizer [46] with $lr = 4 \times 10^{-4}$. For representation learning, we used three NVIDIA TITAN X 24 GB for 360k steps with a total batch size of 30. We trained the L-OGM-only prediction models on a single NVIDIA TITAN RTX 24GB GPU and the multimodal model and batch decoder on two NVIDIA L40 48GB GPUs. The models were trained with a total batch size of 40 until convergence. For the stochastic prediction component, we use a KL annealing with $\beta = 2 \times 10^{-6}$ for the first 10 epochs followed by a linear increase to 0.2 over 50k training steps.

C. Evaluation

Baselines. We benchmark against methods used in L-OGM prediction, such as PredNet [1], [25] and TAAConvLSTM [2]. Additionally, we draw comparisons with state-of-the-art real-time feasible video prediction methods like SimVP V2 [47], PredRNN V2 [48], and E3DLSTM [49]. We also benchmark against a naive baseline that repeats the last observed frame across the entire prediction horizon to assess how effectively the models capture the scene’s motion.

Metric: We evaluate all models using the Image Similarity (IS) metric [50] across the 1.5 s and 3.0 s prediction horizons. For stochastic predictions, we sample 10 predictions and evaluate the best one. IS calculates the smallest Manhattan distance between two grid cells with the same thresholded occupancy, capturing the spatial error of predictions. It determines the grid distance between matrices m_1 and m_2 [50]:

$$\psi(m_1, m_2) = \sum_{c \in \mathcal{C}} d(m_1, m_2, c) + d(m_2, m_1, c) \quad (7)$$

where

$$d(m_1, m_2, c) = \frac{\sum_{m_1[p]=c} \min\{\text{md}(p_1, p_2) | m_2[p_2] = c\}}{\#_c(m_1)} \quad (8)$$

The set of discrete values \mathcal{C} possibly assumed by m_1 or m_2 are: occupied, occluded, and free. $m_1[p]$ denotes the value c of map m_1 at position $p = (x, y)$. $\text{md}(p_1, p_2) = |x_1 - x_2| + |y_1 - y_2|$. $\#_c(m_1) = \#\{p_1 | m_1[p_1] = c\}$ is the number of cells in m_1 with value c .

V. RESULTS

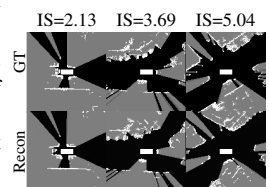
A. Latent Space Analysis

The latent space trained during the representation learning stage is crucial for facilitating accurate predictions. If an agent in the observed frames is lost during the encoding phase, the prediction network struggles to recover this information, leading to incorrect forecasts. We examine the impact of different representation learning losses on reconstruction and prediction performance in Table I. Our results show that incorporating KL and adversarial components decreases reconstruction performance but enhances long-term prediction performance, which is the primary goal. We show randomly selected L-OGMs and their reconstructions in Fig. 4. They demonstrate that the encoder-decoder pairing successfully reconstructs the scene.

TABLE I: The impact of representation learning objective on the reconstruction (\mathbf{IS}_{recon}) and prediction performance ($\mathbf{IS}_{5 \rightarrow X}$) on nuScenes with no augmentation during representation learning. VAE-GAN (KL + Adv) excels at long-term prediction horizon. We also report VAE-GAN performance with the augmented dataset.

Recon	KL	Adv	$\mathbf{IS}_{recon}(\downarrow)$	$\mathbf{IS}_{5 \rightarrow 15}(\downarrow)$	$\mathbf{IS}_{5 \rightarrow 30}(\downarrow)$
No augmentations in representation learning					
✓	×	×	2.18 ± 0.01	7.88 ± 0.16	12.18 ± 0.29
✓	✓	×	5.90 ± 0.01	9.76 ± 0.15	12.69 ± 0.20
✓	×	✓	4.36 ± 0.01	8.36 ± 0.14	11.72 ± 0.21
✓	✓	✓	4.82 ± 0.01	7.94 ± 0.12	10.56 ± 0.17
With augmentations in representation learning					
✓	✓	✓	3.30 ± 0.01	7.00 ± 0.10	9.76 ± 0.16

Fig. 4: Our encoder-decoder effectively reconstructs the L-OGMs, with the IS score reflecting differences in the distribution of occupied cells (e.g., IS of 2.13 and 3.69). In rare instances (e.g., rotation with many agents, IS=5.04), it might lose some detail.



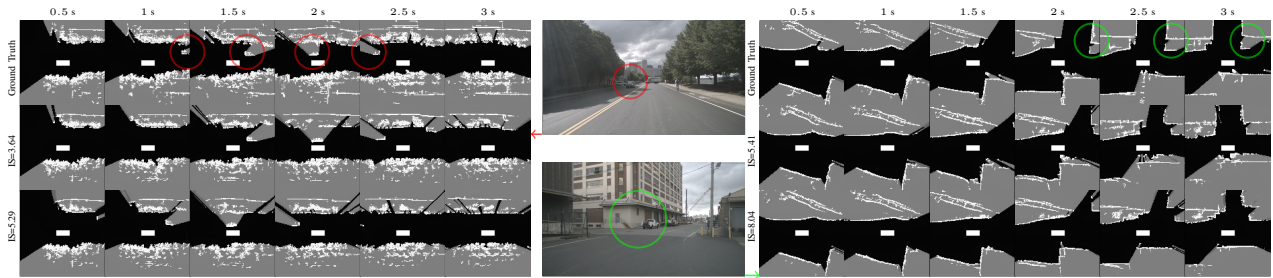


Fig. 5: Examples of LOPR’s prediction samples with visualized front camera observations from the nuScenes dataset. The model is conditioned on all cameras around the vehicle, maps, and the planned trajectory. We report IS scores for each sample. (Left) Prediction of an oncoming vehicle (red) visible only in the front camera. Each sample captures a realistic hypothetical evolution of the scene, such as variations in the velocity of the oncoming car. (Right) Accurate prediction of the static road layout and a parked vehicle (green) visible only in the front camera. Each sample provides a realistic occupancy representation of the parked car and the environment’s layout. Both examples demonstrate that our framework is capable of multi-future reasoning and leveraging multi-modal observations.

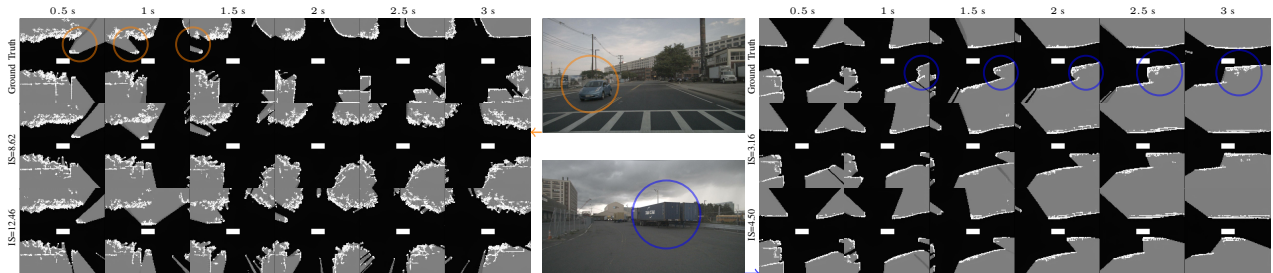


Fig. 6: Examples of LOPR’s prediction samples with visualized front camera from the nuScenes dataset. The prediction setting is the same as in Fig. 5. (Left) Correct forecasting of an oncoming vehicle and static road layout (orange). (Right) Accurate prediction of a parked truck (blue). Each sample captures different velocity of observed car (left) or different shape of static environment (left and right).

B. Prediction Task

General Performance: We compare our framework against the baselines in Table II. The integration of dataset augmentations, stochasticity, additional modalities, and a diffusion decoder each contribute to notable improvements. LOPR outperforms previous methods on both datasets, with improvements becoming more pronounced as the prediction horizon extends. We visualize examples of predictions rolled out for 3.0 s, extending beyond the prediction horizon used during training, in Fig. 5 and Fig. 6. Our framework generates high-quality, realistic predictions, supporting the quantitative results while remaining real-time feasible. It models the multimodal distribution of future agents’ positions and leverages additional modalities to gather information about the surroundings, especially beyond the observable areas in L-OGMs, to make accurate predictions. This includes correctly inferring static parts of the environment, such as road layouts and parked vehicles, as well as dynamic parts, like oncoming vehicles, which are visible in the cameras and maps but not captured in observed L-OGMs (see Fig. 5).

Stochasticity: In challenging scenarios with a lot of partial observability, our framework can infer hypothetical agents. In Fig. 7, we demonstrate this with prediction samples from a model conditioned on L-OGM observations only. Our framework captures different rates of motion of observed agents and infers the entry of a previously unobserved agent. The variational module enables multi-future reasoning about observed and unobserved multi-agent behaviors.

Diffusion-based Decoder: Known weaknesses of mak-

TABLE II: Quantitative evaluation of the prediction performance. Best results are bolded, second-best results are underlined.

Model	NuScenes Dataset		Waymo Open Dataset	
	IS ₅ →15 (↓)	IS ₅ →30 (↓)	IS ₅ →15 (↓)	IS ₅ →30 (↓)
PredRNN V2	30.69±2.10	79.95±4.07	28.45±1.98	62.71±3.38
Sim.VP V2	20.02±1.28	47.20±2.63	15.87±1.18	46.38±2.66
ED3LSTM	10.33±0.29	19.49±0.71	14.36±1.04	36.60±2.15
TAAConvLSTM	7.02±0.17	15.30±0.68	6.71±0.39	21.76±1.56
PredNet	7.10±0.20	14.50±0.52	7.07±0.41	23.88±1.71
Fixed Frame	11.50±0.14	14.41±0.18	10.35±0.41	14.74±0.54
Ours				
Deterministic	7.94±0.13	11.48±0.22	7.62±0.33	12.12±0.73
+ Augmentations	7.24±0.11	10.47±0.19	7.27±0.37	11.81±0.74
+ Stochasticity	7.00±0.10	9.76±0.16	6.64±0.19	9.93±0.28
+ All modalities	<u>6.36±0.08</u>	<u>8.32±0.12</u>	<u>6.23±0.18</u>	<u>9.00±0.28</u>
+ Diffusion Decoder	4.88±0.09	7.12±0.12	5.24±0.18	8.17±0.27

ing predictions in the latent space of generative models include poor temporal consistency and compression losses. We address these concerns with a diffusion-based batch decoder which leads to significant improvements in temporal consistency and the maintenance of detail that is often lost due to compression, as shown in Fig. 8. Numerically, it also results in significant improvements, especially in short-horizon predictions, due to the preservation of static details. However, this comes at the cost of real-time feasibility. While our approach with the single-step decoder and all baselines generate a full sequence of predictions at a rate of 5–10 Hz, decoding predictions with a diffusion decoder takes minutes. Although this leads to significant numerical improvements, most of them do not result in semantically different predictions, making the extra computation time not

worthwhile in most scenarios.

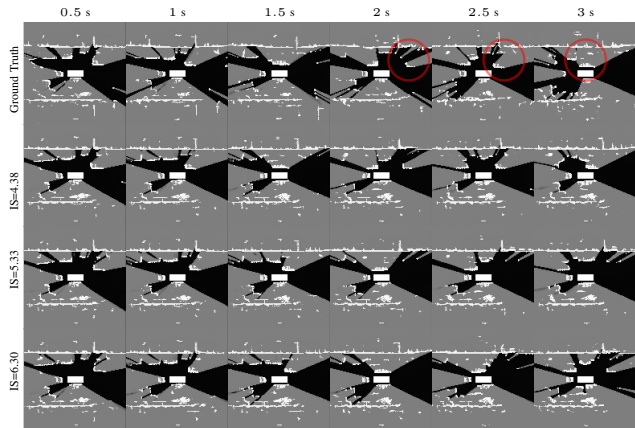


Fig. 7: Visualization of stochastic predictions conditioned solely on L-OGMs, with the IS score averaged over the entire sequence. The scenario captures the motion of numerous agents on the straight road. Our model captures different rates of motion for observed vehicles and can even infer the presence of unobserved ones (red).

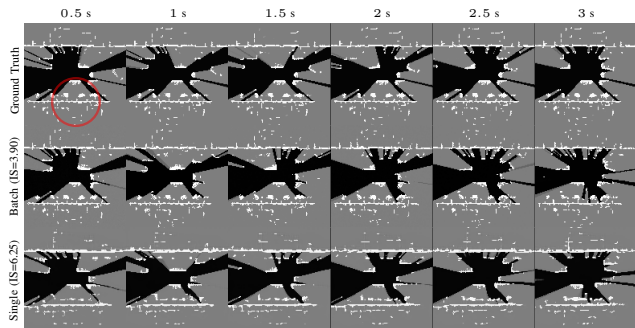


Fig. 8: Visualization of generated predictions decoded with a single-step decoder and further refined with a diffusion-based batch decoder. The batch decoder increases temporal consistency between frames and reduces compression losses. In red, we highlight trees on the side of the road that are recovered with our batch decoder.

Baseline Comparison: The reasons for the significant improvements over prior work are numerous. Prior work is optimized for deterministic prediction tasks in grid cell space and fails to condition on the input modalities available in the autonomous vehicle stack. These methods do not capture the stochastic nature of motion forecasting and lack semantic information about the scene (e.g., distinguishing whether an occupied cell is due to a pedestrian or a sign). As a result, their forecasted L-OGMs gradually lose important details over the prediction horizon, leading to the disappearance of moving objects. While they might capture some static details of the scene, resulting in respectable IS scores for short prediction horizons, they ultimately yield high IS scores as static details vanish and deterministic predictions prove insufficient. Our numerical results demonstrate that the deterministic variation of our framework, conditioned on L-OGMs (the same setting as the baselines), outperforms all baselines over extended prediction horizons. As we incorporate multi-future reasoning, provide additional semantic conditioning, and introduce diffusion decoding, the performance gap between LOPR and the baselines becomes even more substantial, as shown in Table II.

VI. LIMITATIONS

LOPR relies on a well-trained latent space, which may sometimes lose critical details necessary for accurate predictions. If the latent encoding misses important information, the prediction network may not recover it, leading to potentially inaccurate predictions. We have partially addressed this issue with a diffusion decoder. However, this approach may still result in inaccuracies and is not real-time feasible. Additionally, the performance of our framework is heavily influenced by the size of the available perception datasets. The datasets used in this paper contain about six hours of data, which limits performance in scenarios not well-represented in the dataset, such as intersection interactions and cross-traffic.

VII. CONCLUSION

In this paper, we proposed a self-supervised L-OGM prediction framework that captures the stochasticity of the scene and is conditioned on multi-modal observations available in autonomous vehicles. LOPR consists of a VAE-GAN-based generative model that learns an expressive low-dimensional latent space from available sensor modalities, and a transformer-based stochastic prediction network that operates on this learned latent space. Our experiments show that LOPR qualitatively and quantitatively outperforms prior approaches while remaining real-time feasible. We also extend this framework with a diffusion decoder, which addresses temporal consistency issues and mitigates some of the compression losses, albeit at the cost of real-time feasibility. In future work, we will explore extending LOPR to perform 3D occupancy prediction and apply it to other tasks, such as occlusion inference [7], [51] and path planning.

ACKNOWLEDGMENT

This project was made possible by funding from the Ford-Stanford Alliance.

REFERENCES

- [1] M. Itkina, K. Driggs-Campbell, and M. J. Kochenderfer, “Dynamic environment prediction in urban scenes using recurrent representation learning,” in *International Conference on Intelligent Transportation Systems (ITSC)*, IEEE, 2019, pp. 2052–2059.
- [2] B. Lange, M. Itkina, and M. J. Kochenderfer, “Attention augmented ConvLSTM for environment prediction,” in *International Conference on Intelligent Robots and Systems (IROS)*, IEEE, 2020, pp. 1346–1353.
- [3] M. Toyungyernsub, M. Itkina, R. Senanayake, and M. J. Kochenderfer, “Double-prong ConvLSTM for spatiotemporal occupancy prediction in dynamic environments,” in *International Conference on Robotics and Automation (ICRA)*, IEEE, 2021, pp. 13 931–13 937.
- [4] Y. Chai, B. Sapp, M. Bansal, and D. Anguelov, “MultiPath: Multiple probabilistic anchor trajectory hypotheses for behavior prediction,” in *Conference on Robot Learning (CoRL)*, 2020.
- [5] C. Choi, J. H. Choi, J. Li, and S. Malla, “Shared cross-modal trajectory prediction for autonomous driving,” in *cvpr*, 2021, pp. 244–253.
- [6] R. Mahjourian, J. Kim, Y. Chai, M. Tan, B. Sapp, and D. Anguelov, “Occupancy flow fields for motion forecasting in autonomous driving,” *IEEE Robotics and Automation Letters*, vol. 7, no. 2, pp. 5639–5646, 2022.
- [7] B. Lange, J. Li, and M. J. Kochenderfer, “Scene informer: Anchor-based occlusion inference and trajectory prediction in partially observable environments,” in *International Conference on Robotics and Automation (ICRA)*, 2024.

- [8] N. Nayakanti, R. Al-Rfou, A. Zhou, K. Goel, K. S. Refaat, and B. Sapp, "Wayformer: Motion forecasting via simple & efficient attention networks," in *International Conference on Robotics and Automation (ICRA)*, 2023, pp. 2980–2987.
- [9] Y. Chen, B. Ivanovic, and M. Pavone, "Scept: Scene-consistent, policy-based trajectory predictions for planning," in *Computer Society Conference on Computer Vision and Pattern Recognition (CVPR)*, 2022, pp. 17 103–17 112.
- [10] H. Delecki, M. Itkina, B. Lange, R. Senanayake, and M. J. Kochenderfer, "How do we fail? stress testing perception in autonomous vehicles," in *International Conference on Intelligent Robots and Systems (IROS)*, IEEE, 2022, pp. 5139–5146.
- [11] M. Dreissig, D. Scheuble, F. Piewak, and J. Boedecker, "Survey on lidar perception in adverse weather conditions," in *Intelligent Vehicles Symposium (IV)*, 2023.
- [12] A. Elfes, "Using occupancy grids for mobile robot perception and navigation," *Computer*, vol. 22, no. 6, pp. 46–57, 1989.
- [13] M. Schreiber, S. Hoermann, and K. Dietmayer, "Long-term occupancy grid prediction using recurrent neural networks," in *International Conference on Robotics and Automation (ICRA)*, IEEE, 2019, pp. 9299–9305.
- [14] I. Goodfellow, J. Pouget-Abadie, M. Mirza, *et al.*, "Generative adversarial nets," *Advances in Neural Information Processing Systems (NeurIPS)*, vol. 27, 2014.
- [15] D. P. Kingma and M. Welling, "Auto-encoding variational Bayes," *International Conference on Learning Representations (ICLR)*, 2014.
- [16] W. Yan, Y. Zhang, P. Abbeel, and A. Srinivas, "Videoopt: Video generation using vq-vae and transformers," *arXiv preprint arXiv:2104.10157*, 2021.
- [17] A. Hu, L. Russell, H. Yeo, *et al.*, "Gaia-1: A generative world model for autonomous driving," *arXiv preprint arXiv:2309.17080*, 2023.
- [18] H. Caesar, V. Bankiti, A. H. Lang, *et al.*, "NuScenes: A multimodal dataset for autonomous driving," in *Computer Society Conference on Computer Vision and Pattern Recognition (CVPR)*, IEEE, 2020, pp. 11 621–11 631.
- [19] P. Sun, H. Kretzschmar, X. Dotiwalla, *et al.*, "Scalability in perception for autonomous driving: Waymo Open Dataset," in *Computer Society Conference on Computer Vision and Pattern Recognition (CVPR)*, IEEE, 2020, pp. 2446–2454.
- [20] M. Toyungyernsub, E. Yel, J. Li, and M. J. Kochenderfer, "Dynamics-aware spatiotemporal occupancy prediction in urban environments," in *2022 IEEE/RSJ International Conference on Intelligent Robots and Systems (IROS)*, IEEE, 2022, pp. 10836–10841.
- [21] M. Toyungyernsub, E. Yel, J. Li, and M. J. Kochenderfer, "Predicting future spatiotemporal occupancy grids with semantics for autonomous driving," in *Intelligent Vehicles Symposium (IV)*, 2024.
- [22] J. Dequaire, P. Ondruška, D. Rao, D. Wang, and I. Posner, "Deep tracking in the wild: End-to-end tracking using recurrent neural networks," *International Journal of Robotics Research*, vol. 37, no. 4–5, pp. 492–512, 2018.
- [23] M. Schreiber, V. Belagiannis, C. Gläser, and K. Dietmayer, "Dynamic occupancy grid mapping with recurrent neural networks," in *International Conference on Robotics and Automation (ICRA)*, IEEE, 2021, pp. 6717–6724.
- [24] N. Mohajerin and M. Rohani, "Multi-step prediction of occupancy grid maps with recurrent neural networks," in *Computer Society Conference on Computer Vision and Pattern Recognition (CVPR)*, IEEE, 2019, pp. 10 600–10 608.
- [25] W. Lotter, G. Kreiman, and D. Cox, "Deep predictive coding networks for video prediction and unsupervised learning," in *International Conference on Learning Representations (ICLR)*, 2017.
- [26] W. Zheng, W. Chen, Y. Huang, B. Zhang, Y. Duan, and J. Lu, "Occworld: Learning a 3d occupancy world model for autonomous driving," in *Proceedings of the European Conference on Computer Vision (ECCV)*, 2024.
- [27] S. Ettinger, S. Cheng, B. Caine, *et al.*, "Large scale interactive motion forecasting for autonomous driving: The waymo open motion dataset," in *International Conference on Computer Vision (ICCV)*, 2021, pp. 9710–9719.
- [28] C. R. Qi, Y. Zhou, M. Najibi, *et al.*, "Offboard 3d object detection from point cloud sequences," in *Computer Society Conference on Computer Vision and Pattern Recognition (CVPR)*, 2021, pp. 6134–6144.
- [29] X. Tian, T. Jiang, L. Yun, Y. Wang, Y. Wang, and H. Zhao, "Occ3d: A large-scale 3d occupancy prediction benchmark for autonomous driving," in *Advances in Neural Information Processing Systems (NeurIPS)*, 2023.
- [30] G. E. Hinton and R. Zemel, "Autoencoders, minimum description length and Helmholtz free energy," *Advances in Neural Information Processing Systems (NeurIPS)*, vol. 6, 1993.
- [31] A. Van Den Oord, O. Vinyals, *et al.*, "Neural discrete representation learning," in *Advances in Neural Information Processing Systems (NeurIPS)*, vol. 30, 2017.
- [32] D. Ha and J. Schmidhuber, "Recurrent world models facilitate policy evolution," *Advances in Neural Information Processing Systems (NeurIPS)*, vol. 31, 2018.
- [33] M. Babaeizadeh, C. Finn, D. Erhan, R. H. Campbell, and S. Levine, "Stochastic variational video prediction," in *International Conference on Learning Representations (ICLR)*, 2018.
- [34] D. Hafner, T. Lillicrap, J. Ba, and M. Norouzi, "Dream to control: Learning behaviors by latent imagination," in *International Conference on Learning Representations (ICLR)*, 2019.
- [35] S. W. Kim, J. Philion, A. Torralba, and S. Fidler, "DriveGAN: Towards a controllable high-quality neural simulation," in *Computer Society Conference on Computer Vision and Pattern Recognition (CVPR)*, 2021, pp. 5820–5829.
- [36] A. Vaswani, N. Shazeer, N. Parmar, *et al.*, "Attention is all you need," in *Advances in Neural Information Processing Systems (NeurIPS)*, 2017, pp. 5998–6008.
- [37] R. Rakhimov, D. Volkhonskiy, A. Artemov, D. Zorin, and E. Burnaev, "Latent video transformer," in *Proceedings of the International Joint Conference on Computer Vision, Imaging and Computer Graphics Theory and Applications*, 2021.
- [38] M. Oquab, T. Darcet, T. Moutakanni, *et al.*, "Dinov2: Learning robust visual features without supervision," 2024.
- [39] A. B. L. Larsen, S. K. Sønderby, H. Larochelle, and O. Winther, "Autoencoding beyond pixels using a learned similarity metric," in *International Conference on Machine Learning (ICML)*, 2016, pp. 1558–1566.
- [40] R. Zhang, P. Isola, A. A. Efros, E. Shechtman, and O. Wang, "The unreasonable effectiveness of deep features as a perceptual metric," in *Computer Society Conference on Computer Vision and Pattern Recognition (CVPR)*, 2018, pp. 586–595.
- [41] T. Karras, S. Laine, M. Aittala, J. Hellsten, J. Lehtinen, and T. Aila, "Analyzing and improving the image quality of stylegan," in *Computer Society Conference on Computer Vision and Pattern Recognition (CVPR)*, 2020, pp. 8110–8119.
- [42] A. Dosovitskiy, L. Beyer, A. Kolesnikov, *et al.*, "An image is worth 16x16 words: Transformers for image recognition at scale," in *International Conference on Learning Representations (ICLR)*, 2021.
- [43] J. Ho, T. Salimans, A. A. Gritsenko, W. Chan, M. Norouzi, and D. J. Fleet, "Video diffusion models," in *ICLR Workshop on Deep Generative Models for Highly Structured Data*, 2022.
- [44] P. Isola, J.-Y. Zhu, T. Zhou, and A. A. Efros, "Image-to-image translation with conditional adversarial networks," in *Computer Society Conference on Computer Vision and Pattern Recognition (CVPR)*, 2017, pp. 1125–1134.
- [45] P. von Platen, S. Patil, A. Lozhkov, *et al.*, *Diffusers: State-of-the-art diffusion models*, <https://github.com/huggingface/diffusers>, 2022.
- [46] I. Loshchilov and F. Hutter, "Decoupled weight decay regularization," in *International Conference on Learning Representations (ICLR)*, 2019.
- [47] Z. Gao, C. Tan, L. Wu, and S. Z. Li, "Simvp: Simpler yet better video prediction," in *Computer Society Conference on Computer Vision and Pattern Recognition (CVPR)*, 2022, pp. 3170–3180.
- [48] Y. Wang, H. Wu, J. Zhang, *et al.*, "Predrnn: A recurrent neural network for spatiotemporal predictive learning," *IEEE Transactions on Pattern Analysis and Machine Intelligence*, vol. 45, no. 2, pp. 2208–2225, 2022.
- [49] Y. Wang, L. Jiang, M.-H. Yang, L.-J. Li, M. Long, and L. Fei-Fei, "Eidetic 3d lstm: A model for video prediction and beyond," in *International Conference on Learning Representations (ICLR)*, 2019.
- [50] A. Birk and S. Carpin, "Merging occupancy grid maps from multiple robots," *Proceedings of the IEEE*, vol. 94, no. 7, pp. 1384–1397, 2006.
- [51] M. Itkina, Y.-J. Mun, K. Driggs-Campbell, and M. J. Kochenderfer, "Multi-agent variational occlusion inference using people as sensors," in *International Conference on Robotics and Automation (ICRA)*, IEEE, 2022.